

# Plasmon induced brightening of dark exciton in monolayer $WSe_2$ for quantum optoelectronics

Cite as: Appl. Phys. Lett. **114**, 201101 (2019); <https://doi.org/10.1063/1.5093664>  
 Submitted: 23 February 2019 . Accepted: 28 April 2019 . Published Online: 21 May 2019

Ankit Arora , Tejendra Dixit, K. V. Anil Kumar, Sivarama Krishnan, K. Lakshmi Ganapathi, Ananth Krishnan , Pramoda K. Nayak , and M. S. Ramachandra Rao



View Online



Export Citation



CrossMark

## ARTICLES YOU MAY BE INTERESTED IN

[Investigation of the band alignment at  \$MoS\_2/PtSe\_2\$  heterojunctions](#)

Applied Physics Letters **114**, 201601 (2019); <https://doi.org/10.1063/1.5097248>

[Negative refraction inspired polariton lens in van der Waals lateral heterojunctions](#)

Applied Physics Letters **114**, 221101 (2019); <https://doi.org/10.1063/1.5098346>

[Observation of Kerr nonlinearity and Kerr-like nonlinearity induced by terahertz generation in  \$LiNbO\_3\$](#)

Applied Physics Letters **114**, 201102 (2019); <https://doi.org/10.1063/1.5096557>



[WWW.MMR-TECH.COM](http://WWW.MMR-TECH.COM)

**THE WORLD'S RESOURCE FOR  
VARIABLE TEMPERATURE  
SOLID STATE CHARACTERIZATION**



OPTICAL STUDIES SYSTEMS    SUBLUC K SOLIDES SYSTEMS    MICROPROBE STATIONS    HALL EFFECT STUDY SYSTEMS AND MAGNETS

# Plasmon induced brightening of dark exciton in monolayer WSe<sub>2</sub> for quantum optoelectronics

Cite as: Appl. Phys. Lett. **114**, 201101 (2019); doi: [10.1063/1.5093664](https://doi.org/10.1063/1.5093664)

Submitted: 23 February 2019 · Accepted: 28 April 2019 ·

Published Online: 21 May 2019



Ankit Arora,<sup>1,2,3</sup>  Tejendra Dixit,<sup>1,3</sup> K. V. Anil Kumar,<sup>1</sup> Sivarama Krishnan,<sup>1</sup> K. Lakshmi Ganapathi,<sup>1</sup> Ananth Krishnan,<sup>2,a)</sup>  Pramoda K. Nayak,<sup>1,b)</sup>  and M. S. Ramachandra Rao<sup>1,3,c)</sup>

## AFFILIATIONS

<sup>1</sup>Department of Physics and Materials Science Research Centre, Indian Institute of Technology Madras, Chennai 600036, India

<sup>2</sup>Centre for NEMS and Nano Photonics (CNNP), Department of Electrical Engineering, Indian Institute of Technology Madras, Chennai 600036, India

<sup>3</sup>Nano Functional Materials Technology Centre, Indian Institute of Technology Madras, Chennai 600036, India

<sup>a)</sup>Electronic mail: [ananthk@iitm.ac.in](mailto:ananthk@iitm.ac.in)

<sup>b)</sup>Electronic mail: [pnayak@iitm.ac.in](mailto:pnayak@iitm.ac.in)

<sup>c)</sup>Electronic mail: [msrrao@iitm.ac.in](mailto:msrrao@iitm.ac.in)

## ABSTRACT

In the present work, we report plasmon induced brightening of dark excitons ( $X_D$ ) in Au nanoparticle (Au-NP) coated monolayer (1L) WSe<sub>2</sub>. We observed one order enhancement in photoluminescence (PL) intensity and surface enhanced Raman scattering in Au-NP/1L-WSe<sub>2</sub> at room temperature (RT). Temperature dependent PL measurements showed enhanced PL emission from RT down to 100 K in contrast to reduced PL emission which is generally observed for pristine 1L-WSe<sub>2</sub>. We attribute this effect to the out-of-plane electric field induced by the scattering from Au-NPs, which results in the out-of-plane dipole moment and spin-flip of conduction band electrons in Au-NP/1L-WSe<sub>2</sub>, making  $X_D$  bright. Our approach provides a facile way to harness excitonic properties in low-dimensional semiconductors, offering simple strategies for quantum optoelectronics.

Published under license by AIP Publishing. <https://doi.org/10.1063/1.5093664>

Monolayer transition metal dichalcogenides (1L-TMDs), with chemical formula  $MX_2$  ( $M = \text{Mo, W, and so on}$ ;  $X = \text{S, Se, or Te}$ ) are semiconductors with a direct bandgap situated at the K-point of the Brillouin zone.<sup>1,2</sup> These two-dimensional (2D) systems exhibit tightly bound electron-hole pairs called excitons even at room temperature (RT) and therefore have great potential for several photonic applications.<sup>3–5</sup> However, their low quantum efficiency, weak optical absorption, and low photoluminescence (PL) hinder their practical utilization. In the recent past, several methods have been demonstrated to enhance the PL significantly by integrating plasmonic nanostructures with 1L-TMDs.<sup>6–14</sup> The exciton-plasmon interaction in such structures has been discussed in terms of strong near-field enhancement, resonance overlap, and/or charge transfer between plasmonic nanostructures and 1L-TMDs. Surprisingly, the PL enhancement is not unanimous as there are studies reporting both PL enhancement<sup>6,8</sup> and PL quenching<sup>15</sup> in similar systems. The consequence of this process is still under debate and probably needs more comprehensive study of metal/1L-TMD hybrid structures considering other intriguing properties of TMDs.

Due to the absence of inversion symmetry and the presence of strong spin-orbit interaction (SOI), 1L-TMDs show energy bands that exhibit spin splitting with opposite signs in the two valleys<sup>16</sup> as shown in Fig. 1. The magnitude of valence band splitting ( $\Delta_{VB}$ ) is in the range of few hundred millielectron volts, giving rise to two excitonic energy levels labeled as A and B. The conduction band splitting ( $\Delta_{CB}$ ) is in the range of tens of meV, and the spin orientation at the two levels is material dependent.<sup>17–19</sup> Depending on the spin configuration of the electron-hole pair, excitons in 1L-TMD can be either optically bright or dark.<sup>20–22</sup> An exciton is optically bright when it consists of an electron and a hole with opposite spins that exist in the same valley and optically dark otherwise. In the case of 1L-WX<sub>2</sub>, the upper valence band and the lowest conduction band have the same spin in a valley, hence making the lowest intravalley transition optically dark. For MoX<sub>2</sub>, the splitting is opposite to that of WX<sub>2</sub>, i.e., the lowest intravalley transition is optically bright. Dark excitons ( $X_D$ ) exhibit a much longer radiative lifetime compared to bright excitons ( $X_O$ ), which makes them attractive for optically controlled information processing.<sup>23–25</sup> However, optical excitation, detection, and control of  $X_D$

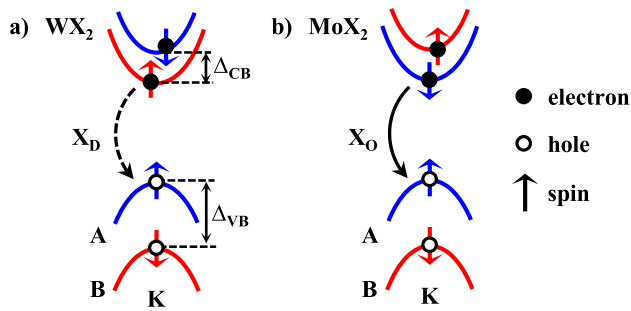


**FIG. 1.** E-k diagram of (a)  $WX_2$  and (b)  $MoX_2$  at the K valley, showing valence band splitting ( $\Delta_{VB}$ ) and conduction band splitting ( $\Delta_{CB}$ ) with the spin orientation.  $X_D$  and  $X_O$  correspond to the optically dark and bright transitions, respectively.

have remained challenging due to their decoupled nature from light.<sup>22,24</sup> Recently, several approaches to couple  $X_D$  with light have been demonstrated by applying either high in-plane magnetic fields<sup>25</sup> or out-of-plane electric fields via near-field coupling to surface plasmon polaritons.<sup>24</sup> In addition to this, Park *et al.* have proposed another method using tip enhanced PL spectroscopy, where a metal nanotip couples to the out-of-plane dipole moment of  $X_D$ , making it bright.<sup>26</sup> These methods are, however, restricted due to the need for cryogenic temperature ( $\sim 4$  K), exceptionally high magnetic field ( $\sim 30$  T), and/or system complexity.

In the present work, we study the exciton-plasmon interaction experimentally by drop-casting Au nanoparticles (Au-NPs) on chemical vapor deposition (CVD) grown 1L-WSe<sub>2</sub>. Temperature dependent PL measurements of these structures showed a gradual increase in PL intensity at reduced temperatures, in contrast to the reduced PL emission observed for pristine 1L-WSe<sub>2</sub>.<sup>27</sup> We attribute this reversed temperature trend of PL intensity in Au-NP/1L-WSe<sub>2</sub> to the brightening of dark excitons. Furthermore, electromagnetic simulations of Au-NP/1L-WSe<sub>2</sub> were carried out to understand this effect. It was observed that some of the scattered components of incident light can give rise to the out-of-plane electric field, which, on the surface of a material with strong SOI, can couple to  $X_D$ , thereby making them bright. This method provides a facile way to optically probe  $X_D$  and manipulate excitonic properties of atomically thin materials, thus opening up new avenues for realizing active metasurfaces and robust quantum optoelectronic systems.

The 1L-WSe<sub>2</sub> flakes were grown on the sapphire substrate using low pressure CVD as mentioned in our earlier report.<sup>28</sup> Colloidal solution of Au-NPs with a mean diameter of  $\sim 45$  nm and the extinction peak at  $\sim 2.3$  eV was prepared using the standard citrate reduction method<sup>29</sup> (shown in Fig. S1, supplementary material). Spherical Au-NPs of this size ( $\sim 50$  nm) were selected in order to have a polarization independent response and a sufficiently high extinction cross-section with a narrow resonance spectrum away from 1L-WSe<sub>2</sub> transition. The synthesized Au-NP solution was drop-cast on as-grown 1L-WSe<sub>2</sub> and dried at 330 K on a hot plate. The atomic force microscopy measurements using a Park Systems NX10 were carried out to determine the flake thickness and Au-NP distribution on 1L-WSe<sub>2</sub> as shown in Fig. S2. PL and the Raman spectroscopy measurements were performed using a HORIBA LabRAM in a confocal microscopy backscattering geometry. Continuous wave (CW) lasers of

energies 1.96 eV and 2.54 eV and optical power  $\sim 700$   $\mu$ W were used as excitation sources. The spot size of these laser beams was  $\sim 1$   $\mu$ m. For RT measurements, a 100 $\times$  objective was used, whereas a 50 $\times$  long working distance objective was used for low temperature measurements down to 100 K.

Figure 2(a) shows the RT-PL spectra of 1L-WSe<sub>2</sub> without and with Au-NPs recorded using an excitation energy of 1.96 eV ( $E_{ex}$ ), which is much below the localized surface plasmon resonance (LSPR) energy of Au-NPs (2.3 eV). This  $E_{ex}$  was selected to avoid any hot-carrier effect or charge transfer between WSe<sub>2</sub> and Au-NPs and to ensure only the near-field enhancement. The PL peak for pristine 1L-WSe<sub>2</sub>/sapphire was observed at  $\sim 1.6$  eV, which is slightly less than that of 1L-WSe<sub>2</sub>/SiO<sub>2</sub>.<sup>30</sup> The PL intensity of Au-NP/1L-WSe<sub>2</sub> was enhanced by an order of magnitude and was blue shifted by  $\sim 20$  meV as compared to pristine 1L-WSe<sub>2</sub>. Since both the excitation and emission energies are far from LSPR, both are expected to be enhanced equally, resulting in overall PL intensity enhancement. The slight blue shift in the peak may be attributed to the change in dipole coupling strength in the vicinity of the enhanced electric field. Figure 2(b) shows the RT Raman spectra of 1L-WSe<sub>2</sub> without and with Au-NPs using  $E_{ex} = 1.96$  eV. Because of the quasi-resonant condition, modes other than the dominant ones were also observed. The Raman spectrum of Au-NP/1L-WSe<sub>2</sub> showed surface enhanced Raman scattering (SERS) due to the near field enhancement. Since there is no alteration in the dominant modes of 1L-WSe<sub>2</sub> [shown in Fig. 2(b)], Au-NPs are expected to be adsorbed physically, indicating no bond formation between 1L-WSe<sub>2</sub> and Au-NPs. The peak at  $\sim 250$   $cm^{-1}$  can be attributed to degenerate  $E'$  and  $A'_1$  modes and at  $\sim 260$   $cm^{-1}$  to the second

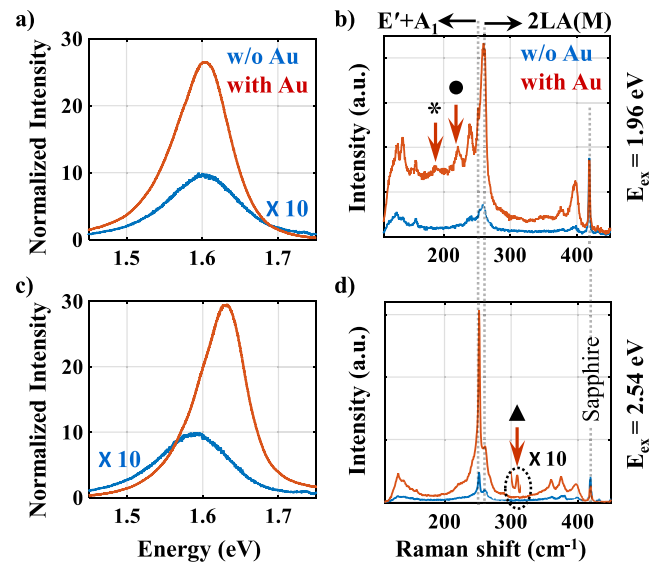


**FIG. 2.** Room temperature (a) and (c) PL and (b) and (d) Raman spectra of 1L-WSe<sub>2</sub> without (blue) and with (red) Au-NPs using 1.96 eV (a) and (b) and 2.54 eV (c) and (d) excitation. For clarity, PL spectra of WSe<sub>2</sub> without Au-NPs are multiplied by a factor of 10. The dominant characteristic Raman modes of 1L-WSe<sub>2</sub> [ $E' + A'_1$  and  $2LA(M)$ ] and the Raman mode of Sapphire are marked with vertical dashed lines. The new emergent peaks are indicated by arrows and marked as \* at  $\sim 180$   $cm^{-1}$  and • at  $\sim 221$   $cm^{-1}$  in (b) and ▲ at  $\sim 308$   $cm^{-1}$  magnified by a factor of 10 in (d).

order 2LA(M) mode. Other peaks present at  $\sim 131\text{ cm}^{-1}$ ,  $139\text{ cm}^{-1}$ ,  $157\text{ cm}^{-1}$ ,  $239\text{ cm}^{-1}$ ,  $375\text{ cm}^{-1}$ , and  $397\text{ cm}^{-1}$  correspond to the higher order and combination modes.<sup>31,32</sup> It can be observed that the intensity of the sapphire peak at  $\sim 418\text{ cm}^{-1}$  remained unaltered as the maximum field enhancement is on the surface of 1L-WSe<sub>2</sub>. In the Raman spectrum of Au-NP/1L-WSe<sub>2</sub>, two new peaks marked as \* at  $\sim 180\text{ cm}^{-1}$  and • at  $\sim 221\text{ cm}^{-1}$  in Fig. 2(b) were observed, which were inactive in pristine 1L-WSe<sub>2</sub>. The peak at  $\sim 221\text{ cm}^{-1}$  corresponds to the combination of LA(M), TA(M), and ZA(M) modes, while the peak at  $\sim 180\text{ cm}^{-1}$  can be attributed to the E'' mode, which is expected at  $\sim 170\text{ cm}^{-1}$  theoretically.<sup>33,34</sup> Interestingly, the E'' mode is forbidden in backscattering experimental geometry,<sup>35</sup> where the light propagation direction is along the *c*-axis of 1L-WSe<sub>2</sub>. It can be expected that due to the enhanced photon scattering by Au-NPs, the E'' mode became active.

The RT PL and Raman spectra of 1L-WSe<sub>2</sub> without and with Au-NPs were also recorded using  $E_{ex} = 2.54\text{ eV}$  as shown in Figs. 2(c) and 2(d). Since  $E_{ex}$  is higher than LSPR of Au-NPs, it can facilitate charge transfer between WSe<sub>2</sub> and Au-NPs. Also, due to the large overlap between  $E_{ex}$  and LSPR, it is expected that the field enhancement of excitation intensity should be more than the emission intensity. However, it was observed that the enhancement in the PL intensity was nearly the same as that with  $E_{ex} = 1.96\text{ eV}$  with a small blue shift ( $\sim 30\text{ meV}$ ). This blue shift may be due to the charge transfer from Au-NPs to 1L-WSe<sub>2</sub>, as WSe<sub>2</sub> is intrinsically p-type in nature.<sup>35,36</sup> The Raman spectrum of Au-NP/1L-WSe<sub>2</sub> showed the emergence of a weak peak at  $\sim 308\text{ cm}^{-1}$  marked as ▲, which may be due to the strong phononic coupling between Au-NPs and 1L-WSe<sub>2</sub>.<sup>37</sup> For comparison, similar studies were carried out on CVD grown 1L-MoS<sub>2</sub>/SiO<sub>2</sub> as shown in Fig. S3. The RT-PL intensity was found to be almost double as compared to pristine MoS<sub>2</sub> for both 1.96 eV and 2.54 eV excitation.

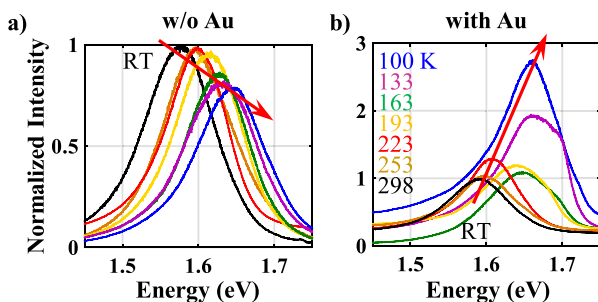
In order to further explore the effect of Au-NPs on the excitonic properties of 1L-WSe<sub>2</sub>, temperature dependent PL measurements were carried out. Figure 3(a) shows the temperature dependent PL spectra of as-grown pristine 1L-WSe<sub>2</sub> in the range of RT to 100 K using  $E_{ex} = 1.96\text{ eV}$ . It was observed that there is a gradual reduction in the PL intensity with the reduction in temperature. This decrease in the PL intensity was due to the fact that the lowest transition in 1L-WSe<sub>2</sub> is optically dark.<sup>27</sup> As discussed above, the lowest energy A exciton in the case of 1L-WSe<sub>2</sub> can be either a spin-forbidden intervalley exciton or a momentum-forbidden intervalley exciton. At RT, due to sufficient thermal energy, there exists some population in the upper

conduction band of 1L-WSe<sub>2</sub>, resulting in an optically bright A exciton which dominates the RT PL. As the temperature decreases, the exciton population at the upper conduction band decreases and the lowest state increases, resulting in PL quenching. The blue shift in the PL with the reduction in temperature was also observed, which can be attributed to the reduction in the phonon scattering. For comparison, temperature dependent PL was also carried out for CVD grown 1L-MoS<sub>2</sub>, where PL intensity was observed to increase with the reduction in temperature because the lowest state is optically bright.<sup>1,20</sup> Therefore, the temperature dependences of the PL intensity of 1L-WSe<sub>2</sub> and 1L-MoS<sub>2</sub> are in clear contrast to each other, demonstrating the existence of the dark exciton in the former, while the bright exciton in the latter (the PL trend shown later in Fig. 4).

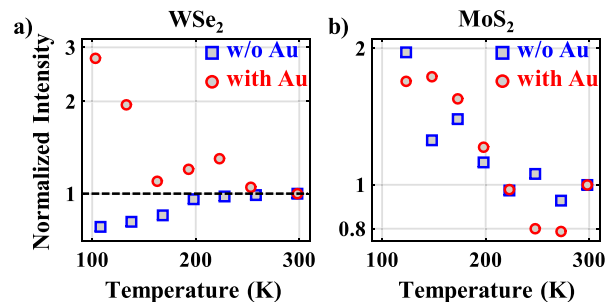
Figure 3(b) shows the temperature dependent PL spectra of Au-NP/1L-WSe<sub>2</sub>, and it was observed that there is an increase in the PL intensity with the reduction in temperature, which was opposite to the temperature dependence of pristine 1L-WSe<sub>2</sub>. The blue shift with the reduction in temperature was the same as that of pristine 1L-WSe<sub>2</sub> (Fig. S4). These measurements were repeated several times for different flakes and were found to exhibit the same trend. Some asymmetry in the PL line shape was observed for low temperatures similar to that reported by Yan *et al.*<sup>38</sup>

Figure 4(a) shows the temperature vs PL intensity of 1L-WSe<sub>2</sub> without and with Au-NPs. The PL intensity at different temperatures has been normalized with respect to that of RT. The horizontal dashed line corresponds to the PL intensity at RT. It is clearly evident that the PL intensity for pristine 1L-WSe<sub>2</sub> lies below the dashed line for all temperatures, while that of the Au-NP/1L-WSe<sub>2</sub> lies above it. The PL intensity of Au-NP/1L-WSe<sub>2</sub> at 100 K was observed to be  $\sim 3$  times more than that at RT. Figure 4(b) shows the temperature vs PL intensity of MoS<sub>2</sub> without and with Au-NPs, where the temperature dependence of intensity remained unaltered, indicating the diversified effect of Au-NP interaction with WSe<sub>2</sub> and MoS<sub>2</sub>.

The effect of Au-NPs, plasmon-exciton interaction, and the field experienced by the exciton is known to remain almost constant over the investigated temperature range.<sup>39</sup> The possible reasons for the reversed trend of the PL intensity vs temperature for Au-NP/1L-WSe<sub>2</sub> include: (i) luminescence from localized/defect states; (ii) emission from intervalley indirect transition; and (iii) perturbation in lowest dark state transition. Localized states originate due to the disorder or defect in the material because of impurity, stress, and/or substrate



**FIG. 3.** Temperature dependent PL spectra of 1L-WSe<sub>2</sub> (a) without and (b) with Au-NPs using 1.96 eV excitation. The direction of the red arrow indicates the reduction in temperature from RT to 100 K. In both the cases, the intensity was normalized with respect to the RT intensity.



**FIG. 4.** (a) Temperature vs PL intensity of 1L-WSe<sub>2</sub> without (blue square) and with (red circle) Au-NPs using 1.96 eV excitation; (b) temperature vs PL intensity of MoS<sub>2</sub> without (blue square) and with (red circle) Au-NPs using 2.54 eV excitation. In both the cases, the intensity was normalized with respect to the RT intensity.

roughness.<sup>40</sup> Emission from these states may also be significantly affected by Au-NPs coated on the flakes.<sup>11</sup> Emission from these states increases with the decrease in temperature and occurs at much lower energy than that of the free exciton. However, localized state emissions are observed at temperatures as low as few tens of Kelvins and become insignificant above 100 K.<sup>11,38,40</sup> In the present experiments, an increase in the intensity was observed for all the temperatures below RT with a consistent blue shift and no emergence of new low energy peaks. Therefore, the contribution from localized states to the reversed temperature trend can be ruled out. Second, the intervalley excitons are momentum-forbidden and need phonon interaction to become optically active. Since the phonon population decreases with the decrease in temperature, the possibility of intervalley excitons can also be eliminated.

Therefore, the only possible reason for this reversed trend can be due to the perturbation in the lowest optically dark-state transition. As discussed previously, there exists conduction band spin splitting in 1L-WSe<sub>2</sub>, which gives rise to the intravalley optically dark state which has recently been shown to consist of two distinct states.<sup>41</sup> Because of the short range electron-hole exchange interaction, the degeneracy of this dark state is lifted. The lower state is spin-forbidden and electric dipole forbidden, known as the perfectly Dark exciton ( $X_{pD}$ ), and the upper state is spin-forbidden but electric-dipole allowed (out-of-plane of the 1L), known as the Gray exciton ( $X_G$ ). These dark states can be made optically bright with the use of the in-plane magnetic field, out-of-plane electric field, and/or reflection symmetry breaking.<sup>42</sup>

In the present work, all the PL measurements were carried out in backscattering geometry, where neither the external in-plane magnetic field nor the out-of-plane electric field was used. However, the Au-NPs have a large scattering cross-section<sup>43,44</sup> and can scatter the incident light to a wide range of angles, some of which would be along the plane of 1L-WSe<sub>2</sub> with an out-of-plane electric field component [schematic shown in Fig. 5(a)]. To verify this, single nanoparticle electromagnetic simulation was carried out using CST-Microwave Studio, a commercial electromagnetic solver<sup>45</sup> (the details are given in Sec. S5). Figure 5(c) shows the simulated time averaged  $e_x$  and  $e_z$  components of the electric field at 1.96 eV. It was observed that, for the x-polarized excitation, the scattered electric field has both the x and z components. In fact, the  $e_z$  component was well confined between the Au-NP and 1L-WSe<sub>2</sub> with strength more than that of  $e_x$  in the vicinity of Au-NP. This out-of-plane  $e_z$  component can be responsible for the brightening of both the components ( $X_G$ ,  $X_{pD}$ ) of dark excitons. The  $X_G$  exciton interacts with  $e_z$  via the out-of-plane electric dipole moment and becomes optically bright. Recently, it has been experimentally demonstrated that  $X_G$  can be excited/detected optically using either in-plane illumination or a high numerical aperture objective lens.<sup>46</sup> Moreover, the  $e_z$  component breaks the reflection symmetry of 1L-WSe<sub>2</sub>. This reflection symmetry breaking along with the strong spin-orbit interaction in 1L-WSe<sub>2</sub> can lead to the spin flip and hence make  $X_{pD}$  bright.<sup>42,47,48</sup> Therefore, Au-NPs in the vicinity of 1L-WSe<sub>2</sub> give rise to the out-of-plane electric field due to the wide angle scattering of the incident light, which was also evident from the emergence of new peaks in the Raman Spectrum of Au-NP/1L-WSe<sub>2</sub>, shown in Fig. 2(b). The PL spectrum of Au-NP/1L-WSe<sub>2</sub> at 100 K was further analyzed by deconvolving into the constituent Gaussian peaks (shown in Fig. S5). The two curves with peaks at 1.71 eV and 1.66 eV can be attributed to  $X_O$  and  $X_D$  respectively, with the peak separation of  $\sim 45$  meV.<sup>17-19</sup>

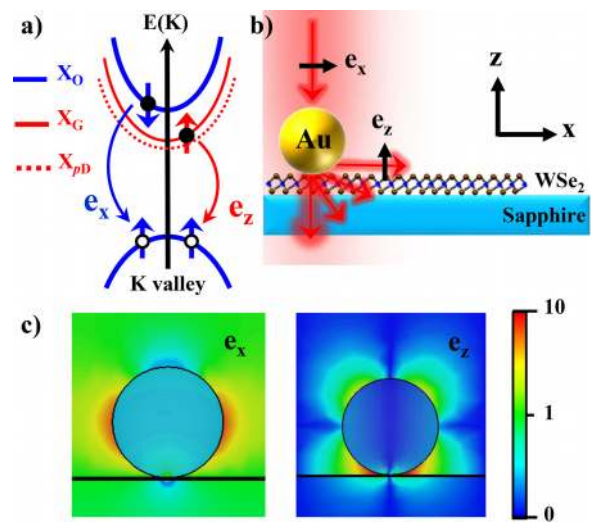


**FIG. 5.** Brightening of the Dark exciton: (a) E-k diagram of 1L-WSe<sub>2</sub> at the K valley, showing conduction band splitting into bright (blue) and dark (red) exciton levels. Furthermore, the fine structure splitting of the dark exciton into lower spin-flip allowed ( $X_{pD}$ ) and upper z-dipolar allowed ( $X_G$ ) is also shown. For clarity, electrons and holes are shown off the central axis and only the A-exciton level is shown in the valence band. (b) Schematic of Au-NP/1L-WSe<sub>2</sub> on Sapphire, showing the wide angle scattering of the x-polarized incident light ( $e_x$ ), resulting in light along the plane of 1L-WSe<sub>2</sub> with the  $e_z$  component. (c) Simulated electric field plot showing the  $e_x$  and  $e_z$  component of electric field distribution on the x-z cross section. The color represents the normalized electric field intensity  $|e/e_o|$  on the log scale.

In conclusion, a reversed temperature trend of PL intensity was observed in Au-NP/1L-WSe<sub>2</sub> structures, which could be assigned to the brightening of  $X_D$ . Scattering from Au-NPs resulted in an out-of-plane electric field, which was supported by single NP electromagnetic simulation. The combined effect of this out-of-plane electric field and strong SOI in 1L-WSe<sub>2</sub> resulted in brightening of  $X_D$ . This work provides a simple approach for tuning excitonic properties of atomically thin materials, offering simple strategies for quantum optoelectronics. This work also indicates that the effect of plasmon-exciton interaction can have far-reaching consequences due to intriguing properties of materials and not just a result of field enhancement and charge transfer.

See the [supplementary material](#) for Au-NP characterization; AFM images of 1L-WSe<sub>2</sub>; PL spectra of MoS<sub>2</sub>; and deconvolved PL spectra of Au-NP/1L-WSe<sub>2</sub> showing  $X_D$ .

This work was partially supported by the Department of Science and Technology India (DST) that led to the establishment of the Nano Functional Materials Technology Centre (Grant No. SR/325NM/NAT/02-2005). P.K.N. acknowledges the financial support from DST (Grant No. SERB/F/5379/2017-2018, Ramanujan Fellowship). K.L.G. acknowledges the financial support from DST (Grant No. DST/INSPIRE/04/2016/001865, INSPIRE Faculty program).

## REFERENCES

- <sup>1</sup>K. F. Mak, C. Lee, J. Hone, J. Shan, and T. F. Heinz, *Phys. Rev. Lett.* **105**, 136805 (2010).

- <sup>2</sup>A. Splendiani, L. Sun, Y. Zhang, T. Li, J. Kim, C.-Y. Chim, G. Galli, and F. Wang, *Nano Lett.* **10**, 1271 (2010).
- <sup>3</sup>K. He, N. Kumar, L. Zhao, Z. Wang, K. F. Mak, H. Zhao, and J. Shan, *Phys. Rev. Lett.* **113**, 026803 (2014).
- <sup>4</sup>T. Mueller and E. Malic, *npj 2D Mater. Appl.* **2**, 29 (2018).
- <sup>5</sup>S. Z. Butler, S. M. Hollen, L. Cao, Y. Cui, J. A. Gupta, H. R. Gutiérrez, T. F. Heinz, S. S. Hong, J. Huang, A. F. Ismach *et al.*, *ACS Nano* **7**, 2898 (2013).
- <sup>6</sup>Z. Wang, Z. Dong, Y. Gu, Y.-H. Chang, L. Zhang, L.-J. Li, W. Zhao, G. Eda, W. Zhang, G. Grinblat *et al.*, *Nat. Commun.* **7**, 11283 (2016).
- <sup>7</sup>F. Cheng, A. D. Johnson, Y. Tsai, P.-H. Su, S. Hu, J. G. Ekerdt, and C.-K. Shih, *ACS Photonics* **4**, 1421 (2017).
- <sup>8</sup>K. C. Lee, Y.-H. Chen, H.-Y. Lin, C.-C. Cheng, P.-Y. Chen, T.-Y. Wu, M.-H. Shih, K.-H. Wei, L.-J. Li, and C.-W. Chang, *Sci. Rep.* **5**, 16374 (2015).
- <sup>9</sup>S. Najmaei, A. Mlayah, A. Arbouet, C. Girard, J. Léotin, and J. Lou, *ACS Nano* **8**, 12682 (2014).
- <sup>10</sup>J. Kern, A. Trügler, I. Niehues, J. Ewering, R. Schmidt, R. Schneider, S. Najmaei, A. George, J. Zhang, J. Lou, U. Hohenester, S. M. de Vasconcelos, and R. Bratschitsch, *ACS Photonics* **2**(9), 1260–1265 (2015).
- <sup>11</sup>A. D. Johnson, F. Cheng, Y. Tsai, and C.-K. Shih, *Nano Lett.* **17**, 4317 (2017).
- <sup>12</sup>B. Mukherjee, N. Kaushik, R. P. Tripathi, A. Joseph, P. Mohapatra, S. Dhar, B. Singh, G. P. Kumar, E. Simsek, and S. Lodha, *Sci. Rep.* **7**, 41175 (2017).
- <sup>13</sup>J. Yan, C. Ma, P. Liu, and G. Yang, *ACS Photonics* **4**, 1092 (2017).
- <sup>14</sup>J. Sun, H. Hu, D. Zheng, D. Zhang, Q. Deng, S. Zhang, and H. Xu, *ACS Nano* **12**, 10393 (2018).
- <sup>15</sup>U. Bhanu, M. R. Islam, L. Tetard, and S. I. Khondaker, *Sci. Rep.* **4**, 5575 (2014).
- <sup>16</sup>Z. Zhu, Y. Cheng, and U. Schwingenschlögl, *Phys. Rev. B* **84**, 153402 (2011).
- <sup>17</sup>Z. Ye, T. Cao, K. O'Brien, H. Zhu, X. Yin, Y. Wang, S. G. Louie, and X. Zhang, *Nature* **513**, 214 (2014).
- <sup>18</sup>A. Chernikov, T. C. Berkelbach, H. M. Hill, A. Rigosi, Y. Li, O. B. Aslan, D. R. Reichman, M. S. Hybertsen, and T. F. Heinz, *Phys. Rev. Lett.* **113**, 076802 (2014).
- <sup>19</sup>K. Kośmider, J. W. González, and J. Fernández-Rossier, *Phys. Rev. B* **88**, 245436 (2013).
- <sup>20</sup>D. Y. Qiu, H. Felipe, and S. G. Louie, *Phys. Rev. Lett.* **111**, 216805 (2013).
- <sup>21</sup>X. Xu, W. Yao, D. Xiao, and T. F. Heinz, *Nat. Phys.* **10**, 343 (2014).
- <sup>22</sup>J. Echeverry, B. Urbaszek, T. Amand, X. Marie, and I. Gerber, *Phys. Rev. B* **93**, 121107 (2016).
- <sup>23</sup>K. P. Loh, *Nat. Nanotechnol.* **12**, 837 (2017).
- <sup>24</sup>Y. Zhou, G. Scuri, D. S. Wild, A. A. High, A. Dibos, L. A. Jauregui, C. Shu, K. De Greve, K. Pistunova, A. Y. Joe *et al.*, *Nat. Nanotechnol.* **12**, 856 (2017).
- <sup>25</sup>X.-X. Zhang, T. Cao, Z. Lu, Y.-C. Lin, F. Zhang, Y. Wang, Z. Li, J. C. Hone, J. A. Robinson, D. Smirnov *et al.*, *Nat. Nanotechnol.* **12**, 883 (2017).
- <sup>26</sup>K.-D. Park, T. Jiang, G. Clark, X. Xu, and M. B. Raschke, *Nat. Nanotechnol.* **13**, 59 (2018).
- <sup>27</sup>X.-X. Zhang, Y. You, S. Y. F. Zhao, and T. F. Heinz, *Phys. Rev. Lett.* **115**, 257403 (2015).
- <sup>28</sup>P. K. Nayak, Y. Horbatenko, S. Ahn, G. Kim, J.-U. Lee, K. Y. Ma, A.-R. Jang, H. Lim, D. Kim, S. Ryu *et al.*, *ACS Nano* **11**, 4041 (2017).
- <sup>29</sup>J. Turkevich, P. C. Stevenson, and J. Hillier, *Discuss. Faraday Soc.* **11**, 55 (1951).
- <sup>30</sup>M. Dau, C. Vergnaud, A. Marty, F. Rortais, C. Beigné, H. Boukari, E. Bellet-Amalric, V. Guigoz, O. Renault, C. Alvarez *et al.*, *Appl. Phys. Lett.* **110**, 011909 (2017).
- <sup>31</sup>W. Zhao, Z. Ghorannevis, K. K. Amara, J. R. Pang, M. Toh, X. Zhang, C. Kloc, P. H. Tan, and G. Eda, *Nanoscale* **5**, 9677 (2013).
- <sup>32</sup>X. Zhang, X.-F. Qiao, W. Shi, J.-B. Wu, D.-S. Jiang, and P.-H. Tan, *Chem. Soc. Rev.* **44**, 2757 (2015).
- <sup>33</sup>H. Sahin, S. Tongay, S. Horzum, W. Fan, J. Zhou, J. Li, J. Wu, and F. Peeters, *Phys. Rev. B* **87**, 165409 (2013).
- <sup>34</sup>E. del Corro, A. Botello-Méndez, Y. Gillet, A. L. Elias, H. Terrones, S. Feng, C. Fantini, D. Rhodes, N. Pradhan, L. Balicas *et al.*, *Nano Lett.* **16**, 2363 (2016).
- <sup>35</sup>J. Kang, S. Tongay, J. Zhou, J. Li, and J. Wu, *Appl. Phys. Lett.* **102**, 012111 (2013).
- <sup>36</sup>H. Fang, S. Chuang, T. C. Chang, K. Takei, T. Takahashi, and A. Javey, *Nano Lett.* **12**, 3788 (2012).
- <sup>37</sup>M.-H. Chiu, M.-Y. Li, W. Zhang, W.-T. Hsu, W.-H. Chang, M. Terrones, H. Terrones, and L.-J. Li, *ACS Nano* **8**, 9649 (2014).
- <sup>38</sup>T. Yan, X. Qiao, X. Liu, P. Tan, and X. Zhang, *Appl. Phys. Lett.* **105**, 101901 (2014).
- <sup>39</sup>I. Abid, W. Chen, J. Yuan, A. Bohloul, S. Najmaei, C. Avendano, R. Pe?chou, A. Mlayah, and J. Lou, *ACS Photonics* **4**, 1653 (2017).
- <sup>40</sup>S. Zhang, C.-G. Wang, M.-Y. Li, D. Huang, L.-J. Li, W. Ji, and S. Wu, *Phys. Rev. Lett.* **119**, 046101 (2017).
- <sup>41</sup>C. Robert, T. Amand, F. Cadiz, D. Lagarde, E. Courtade, M. Manca, T. Taniguchi, K. Watanabe, B. Urbaszek, and X. Marie, *Phys. Rev. B* **96**, 155423 (2017).
- <sup>42</sup>A. Slobodeniuk and D. Basko, *2D Mater.* **3**, 035009 (2016).
- <sup>43</sup>C. F. Bohren and D. R. Huffman, *Absorption and Scattering of Light by Small Particles* (John Wiley & Sons, 2008).
- <sup>44</sup>U. Kreibitz and M. Vollmer, *Optical Properties of Metal Clusters* (Springer Science & Business Media, 2013), Vol. 25.
- <sup>45</sup>M. Studio, <http://www.cst.com/products/cstmws> for Cst-computer simulation technology (2016).
- <sup>46</sup>G. Wang, C. Robert, M. Glazov, F. Cadiz, E. Courtade, T. Amand, D. Lagarde, T. Taniguchi, K. Watanabe, B. Urbaszek *et al.*, *Phys. Rev. Lett.* **119**, 047401 (2017).
- <sup>47</sup>E. I. Rashba, *Physica E* **20**, 189 (2004).
- <sup>48</sup>J. Ibañez-Azpiroz, A. Eiguren, E. Y. Sherman, and A. Bergara, *Phys. Rev. Lett.* **109**, 156401 (2012).